Applied Mechanics and Materials Vol. 461 (2014) pp 22-30 *Online: 2013-11-21*

doi:10.4028/www.scientific.net/AMM.461.22

Acoustic Performance Analysis of Bionic Coupling Multi-layer Structure

Yonghua Wang[1,2,a], Chengchun Zhang[1,b*], Luquan Ren[1,c],
Mohamed Ichchou[2], Marie-Annick Galland[3], Olivier Bareille[2]

[1]Key Laboratory of Bionic Engineering (Ministry of Education), Jilin University, Changchun 130022, P. R. China

[2]Laboratory of Tribology and System Dynamics, Ecole Centrale de Lyon, Ecully 69134, France

[3]Laboratory of Fluid Mechanics and Acoustics, Ecole Centrale de Lyon, Ecully 69131, France

[a]Yonghua.Wang@ec-lyon.fr, [b*]jluzcc@jlu.edu.cn, [c]lqren@jlu.edu.cn

Keywords: Biomimetic method; Multi-layer acoustic structure; Impedance transfer method; Absorption coefficients

Abstract. The interest of this paper lies in the proposition of using bionic method to develop a new sound absorption structure. Inspired by the coupling absorption structure of the skin and feather of a typical silent flying bird – owl, a bionic coupling multi-layer structure model is developed, which is composed of a micro-silt plate, porous fibrous material and a flexible micro-perforated membrane backed with airspace. The impedance transfer method is applied to calculate the absorption coefficients and analyze the influences of different parameters of each layer on absorption coefficients of this model. Based on numerical simulations, the effectiveness of this proposed model is tested. The average absorption coefficient reaches 0.85 within the frequency range from 200 Hz to 2000 Hz. The significant improvement of absorption coefficients can be mainly due to the Helmholtz effects of the micro-silt plate and flexible micro-perforated membrane, and the combination with porous materials can lead to even better absorption performance in broadband.

Introduction

In recent years, noise control has attracted much attention for improving living environments. Multi-layer acoustic absorbers composed of perforated plates, airspaces and porous materials are commonly applied to absorb broadband noise. However, the acoustic absorption of these multi-layer acoustic absorbers is mainly dependent on their fabrication. In this paper, a new absorption structure is developed through biomimetic method, and the factors that have significant influence on the acoustic absorption performance are analyzed.

Biology has perfected its designs and formed many fruitful abilities through billions of years' evolution. Efficient and reliable technologies and achievements can be developed by adopting the features of natural creations [1-5]. The owl, as observed today, has passed through series of evolution for over 12 million years. It is suggested that the owl has developed its strategy of a silent predator based on various characteristics of its body surface. At present, in the field of bionics, investigations on the noise reduction characteristics of owl body surface are mainly focused on its morphological features. Through comparative experiments on morphological characteristics of owl's wing surface, Graham [6] revealed that its special wing feathers had a significant impact on noise reduction capacity. Based on pneumatic noise test during the predation process of striped owl, Kroeger *et al.* [7] found that the primary feather edge was indented, which was conducive to noise suppression and even influenced its physical trajectory. Through long-term observation and experiments, Lilley *et al.* [8] proposed following tentative but plausible reasons for the reduction and suppression of noise: (1) leading edge of primary feathers in the form of a comb, (2) trailing edge feathers in the form of a fringe, and (3) fluffy down on the wings, abdomen, legs and tarsus. In 2004, Lilley [9] attempted to optimize the take-off and landing of quiet commercial passenger transport according to the noise

reduction characteristics of owl body surface and obtained satisfactory results. Ren *et al.* [10, 11] considered that the skin and feather of owl chest and abdominal may also play an important role on its silent flight. It was concluded that the noise suppression of the owl chest and abdominal was due to the synergy effect of material, skin structure and feather shape etc., and further named as biological coupling. Inspired by this fact, a bionic coupling multi-layer structure is established in this article according to the bionic analogy principle.

Davern [12] presented an experimental study on a three-layer assembly which contained perforated plate, porous material and airspace. Dunnand and Davern [13] proposed an analytical analysis for the flat-walled anechoic lining composed of outer, middle and inner layer porous materials. Jinkyo *et al.* [14] further studied the assembly with two layers of perforated plates backed with airspaces by an equivalent electrical circuit method (EECM). Chen *et al.* [15] applied finite element method (FEM) to analyze the acoustic absorption of porous materials with different surface shapes and perforated plates. Lin *et al.* [16] provided a detailed investigation of the impact of porous materials with different thickness and configuration on the perforated plate. Lee *et al.* [17] estimated the absorption performance of multiple layer perforated plate systems by transfer matrix method (TMM). Lee and Chen [18] proposed acoustic transmission analysis method to analyze the absorption of multi-layer absorber, which was subsequently developed into the impedance transfer method (ITM). Zhao *et al.* [19] compared EECM, ITM and TMM, and proved that ITM and TMM were essentially the same and more accurate than EECM. Accordingly, ITM is selected among all the methods for the analyses in this study.

Materials and Methods

Establishment of the bionic model. Ren [10] investigated the acoustic performance of the chest and abdominal skin and feather samples of long-eared owl, pheasant and pigeon. Some bionic characteristics of long-eared owl are displayed in Fig. 1 (a. ribbed structure of feather surface, b. micro-slit structure of feather, c. fibrous structure of fluff, d. cavity under the dermal layer of skin). The absorption comparison of different bird samples is shown in Fig. 2.

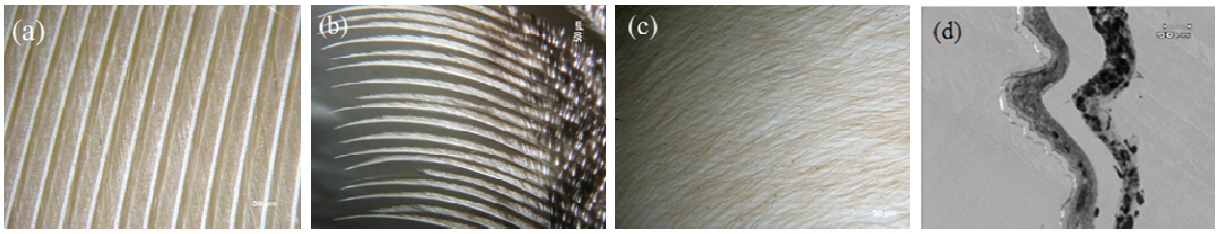

Fig. 1 Some bionic characteristics of long-eared owl

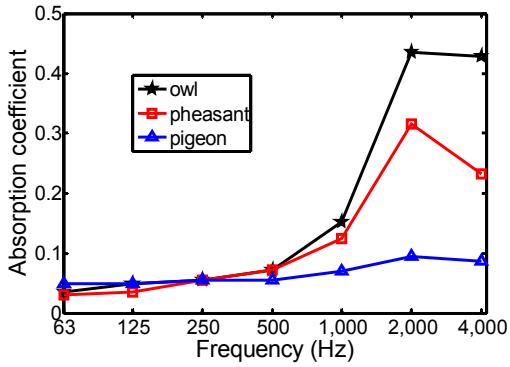

Fig. 2 Absorption comparison of different bird samples

Fig. 2 indicates that the absorption coefficients of owl skin and overlying feathers are much higher than the other two birds, especially within the frequency range from 1000 Hz to 4000 Hz. In the present study, bionic coupling modeling method is used to analyze the surface noise reduction

mechanism based on the absorption characteristics of long-eared owl. The bionic analogies are characterized as follows: (1) The covering feather is analogous to rigid micro-slit plate. (2) The chest fluff is analogous to uniform fiber absorption material. (3) The dermis layer and subcutaneous cavity are analogous to a sound absorber composed of flexible micro-perforated membrane and airspace. The bionic coupling structure (a) and some comparative models (b) are shown in Fig. 3. Fig. 3b is composed of model 1 (a micro-slit plate backed with airspace), model 2 (a micro-slit plate backed with porous material), model 3 (double layer structure of micro-slit plate and micro-perforated membrane), model 4 (multi-layer structure of micro-slit plate, porous material and airspace), and model 5 (multi-layer structure of micro-slit plate, porous material, micro-perforated membrane and airspace). The first four are contrast models and the fifth is the bionic model.

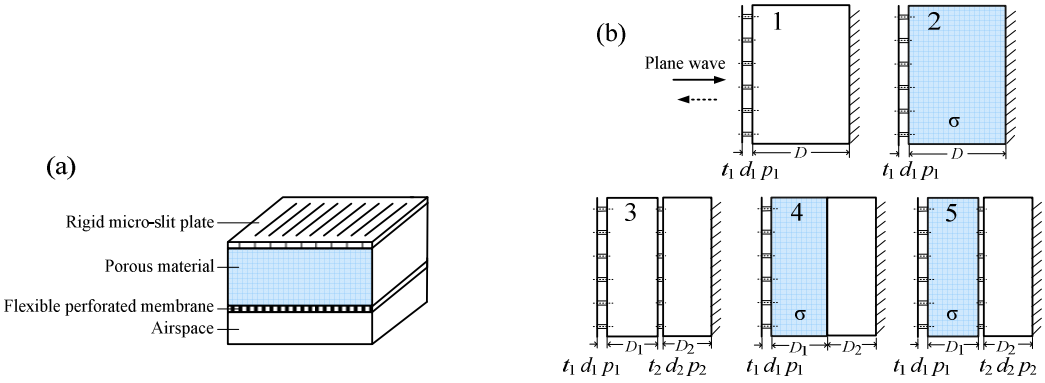

Fig. 3 The bionic absorption structure and comparative models

Calculation method of absorption performance. The methods used to analyze the various absorption performances in the study are discussed in following sections.

Acoustic impedance of rigid micro-silt plate. The calculation of acoustic performance of micro-slit plate is based on Maa's micro-silt theory [20] and expresses in Eq. (1-2).

$$Z_p = \frac{12\eta t}{p\rho_0 c_0}\left(1+\frac{x^2}{18}\right)^{0.5} + \frac{j\omega t}{pc_0}\left[1+(25+2x^2)^{-0.5}\right] \tag{1}$$

$$Z_D = -j\rho_0 c_0 \cdot \cot\left(\frac{\omega D}{c_0}\right) \tag{2}$$

Where, $\omega=2\pi f$ is the angular frequency, f is the frequency, $x = 0.5d\sqrt{\omega/\mu}$ is the perforated constant, $j=\sqrt{-1}$, t, d, p $(=\pi d^2/b^2)$ are the thickness, width of micro-slit and porosity of micro-slit plate, respectively, b is the distance between two adjacent pores, η, ρ_0, c_0 are the kinematic viscosity of air, density of air and sound speed, D is the thickness of the airspace behind the micro-slit plate, Z_P and Z_D are the impedances of micro-slit plate and airspace.

Acoustic impedance of porous material. Considering the accuracy and simplicity, Delany – Bazley – Miki [21] model is proposed to evaluate the wavenumber k and characteristic impedance Z_c (Eq. 3-5).

$$Z_c = \rho_0 c_0\left[1+5.50\left(10^3\frac{f}{\sigma}\right)^{-0.632} - j8.43\left(10^3\frac{f}{\sigma}\right)^{-0.632}\right] \tag{3}$$

$$k = \frac{\omega}{c_0}\left[1+7.81\left(10^3\frac{f}{\sigma}\right)^{-0.618} - j11.41\left(10^3\frac{f}{\sigma}\right)^{-0.618}\right] \tag{4}$$

$$\text{For} \quad 0.01 < \frac{f}{\sigma} < 1.00 \tag{5}$$

Where, σ is the resistivity of porous material.

Acoustic impedance of flexible micro-perforated membrane. A micro-perforated membrane backed by airspace makes a resonant system, which can be obtained using the impedance type of electro-acoustic analogy. Basically, the resonant system contains the mass-resistance element in series with the cavity reactance of the airspace. Single layer of micro-perforated membrane and its equivalent circuit [22] are shown in Fig. 4. The acoustic performance can be represented by Eq. (6-12).

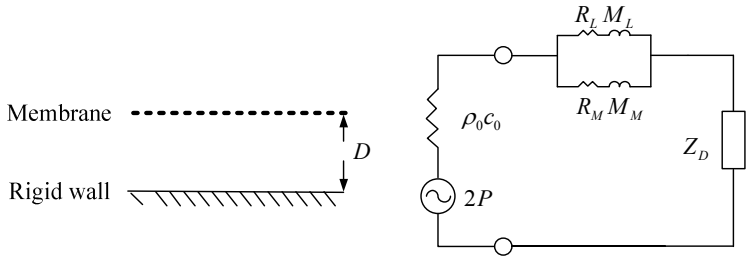

Fig. 4 Single layer of micro-perforated membrane and its equivalent circuit

$$Z_M = R_M + jM_M = \rho_0 c_0 (r' + j\omega m'') \tag{6}$$

$$Z_L = R_L + jM_L = \rho_0 c_0 (r + j\omega m) \tag{7}$$

$$r = \frac{g_1 t}{p d^2}\left[\left(1+\frac{x^2}{32}\right)^{0.5} + \frac{\sqrt{2}x}{8}\cdot\frac{d}{t}\right] \tag{8}$$

$$m = \frac{t}{p c_0}\left[1+\left(9+\frac{x^2}{2}\right)^{-0.5} + 0.85\frac{d}{t}\right] \tag{9}$$

$$Z = Z_p + Z_D = \frac{Z_M Z_L}{Z_M + Z_L} + Z_D = \rho_0 c_0 \left[H_r + j\left(H_m - \cot(\omega D / c_0)\right)\right] \tag{10}$$

With

$$H_r = \frac{\left(rr' - \omega^2 mm''\right)\times\left(r+r'\right) + \left(r'\omega m - rmm''\right)\times\left[\omega(m+m'')\right]}{\left(r+r'\right)^2 + \left[\omega(m+m'')\right]^2} \tag{11}$$

$$H_m = \frac{\left(r'\omega m - rmm''\right)\times\left(r+r'\right) + \left(rr' - \omega^2 mm''\right)\times\left[\omega(m+m'')\right]}{\left(r+r'\right)^2 + \left[\omega(m+m'')\right]^2} \tag{12}$$

Where, R_M and M_M are the specific acoustic resistance and reactance of the membrane, R_L and M_L are the specific acoustic resistance and reactance of the apertures, $x = g_2 d\sqrt{f}$ is the perforated constant, m' is the surface density of the membrane (kg/m^2), $m'' = m'/\rho_0 c_0$ is the surface density of the membrane (kg/m^2), r' is the normalized specific acoustic resistance of the membrane, which mainly depends on mounting conditions. For a non-metallic material, g_1=0.147 and g_2= 0.316. For a metallic material, g_1=0.335 and g_2=0.21.

Acoustic impedance of multi-layer absorber. The generalization of ITM [18] for a multi-layer structure is shown in Fig. 5. In case of the first compartment of the multi-layer structure, surface acoustic impedance Γ_{j1} of the first layer (airspace or porous material) can be represented by Eq. (13).

$$\Gamma_{j1} = Z_{cj1}\frac{Z_r \cot(k_{j1}t_{j1}) + Z_{cj1}}{Z_r + Z_{cj1}\cot(k_{j1}t_{j1})} \tag{13}$$

Where, Z_r is the back surface acoustic impedance of the first compartment, and it is backed with a rigid wall and taken as ∞, Z_{cj1} is the characteristic impedance of the layer considered for airspace or porous material. Similarly, the surface acoustic impedance of the next layer of airspaces or porous materials can also be evaluated by Eq. (13). However, the back surface acoustic impedance Z_r is substituted by the surface acoustic impedance Γ_{j1} for the subsequent layer. Thus, the effects of various combinations of airspaces and porous materials between adjacent perforated plates can be accurately described.

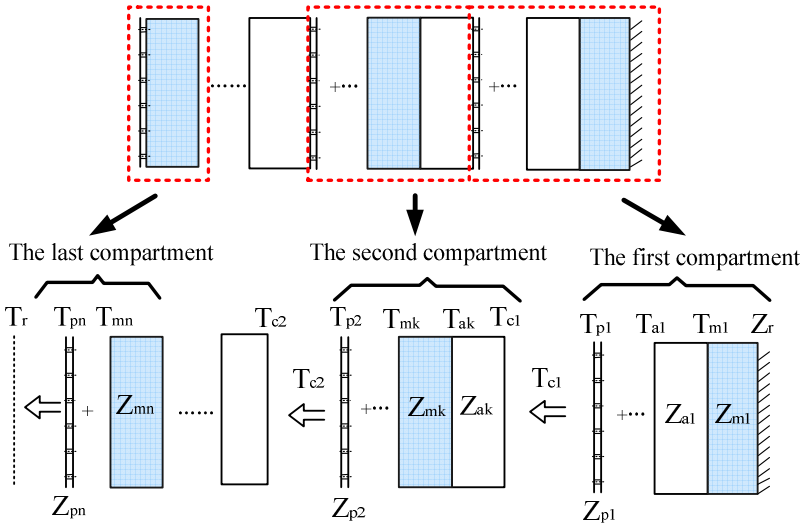

Fig. 5 Generalization of ITM for a multi-layer structure

The surface acoustic impedance Γ_{c1} for the first compartment can be evaluated by the surface acoustic impedance of the first layer of perforated plate Z_{P1} and the k-1 layer of airspace or porous material $\Gamma_{j(k-1)}$ as Eq. (14).

$$\Gamma_{c1} = Z_{p1} + \Gamma_{j(k-1)} \tag{14}$$

In case of the subsequent calculation, the surface acoustic impedance Γ_{c1} for the first compartment can be treated as the back surface acoustic impedance of the first layer of the second compartment. Consequently, the resultant surface acoustic impedance Γ_r of the practical multi-layer acoustic absorber can be evaluated by ITM.

Absorption coefficients of the multi-layer absorber. The absorption coefficients α of the multi-layer structure can be calculated by Eq. (15).

$$\alpha = \frac{4Re\left(\Gamma_r / Z_0\right)}{\left[1 + Re\left(\Gamma_r / Z_0\right)\right]^2 + \left[Im\left(\Gamma_r / Z_0\right)\right]^2} \tag{15}$$

Where, $Z_0 = \rho_0 c_0$ is the characteristic impedance of air, Γ_r is the total acoustic impedance of the multi-layer absorber.

Results and discussion

Validation of the results. The comparisons of absorption coefficients of micro-perforated membranes (a), double layer micro-perforated plate (b – model 3) and multi-layer acoustic absorbers (c – model 4) are shown in Fig. 7. The parameters of membrane 1 are: $m^{'}$=0.19 kg/m^2, t=0.17 mm, l=0.06 mm, p=0.83%, membrane 2 with $m^{'}$=0.13 kg/m^2, t=0.13 mm, l=0.18 mm, p=4.7%, model 3 with $d_1 = d_2$=0.8 mm, $t_1 = t_2$=0.8 mm, $p_1 = p_2$=0.03, D_1=32 mm, D_2=23 mm and model 4 with t_1=6.3 mm, p_1=4.7%, $D_1 = D_2$=25 mm. The experiment datas of micro-perforated membranes and model 4 are provided by Kang [22] and Davern [23], respectively. The results indicate that the

calculation method of micro-perforated membrane and ITM agree reasonably well with the experimental data for the all the structures. Thus, the methods described in section 2.2 are validated for the study of acoustic characteristics of the models.

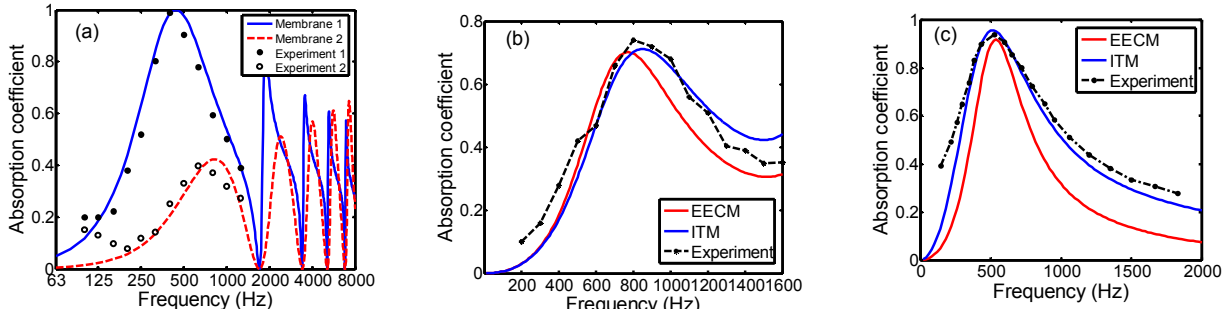

Fig. 6 Comparisons of absorption coefficients of different absorption structures

Absorption performance of the bionic model. The parameters of the bionic model are determined according to the size of bionic characteristics of long-eared owl. With reference to Fig. 3b, the various parameters considered are: t_1=2 mm, d_1=0.5 mm, p_1=5%, t_2=0.2 mm, d_2=0.06 mm, p_2=0.83%, m'=0.19 kg/m2, D_1=25 mm, σ =10000 $Pa \cdot s / m$, D_2=25 mm and $D = D_1 + D_2$=50 mm. The comparison of absorption coefficients of the various models are shown in Fig. 7. The results suggest that the micro-slit plate filled with porous material considerably improves the absorption coefficients (model 1 and 2, model 1 and 4). The double layer micro-perforated plate broadens the absorption band (model 1 and 3, model 4 and 5). The bionic model (model 5) has best absorption capacity without increasing the total thickness, and its average absorption coefficient reaches 0.85 within the frequency range from 200 Hz to 2000 Hz.

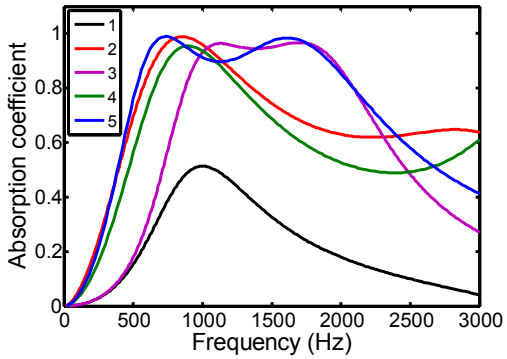

Fig. 7 Comparison of absorption coefficients of the various models

Optimization of parameters for the bionic model. The influences of different parameters for each layer of the bionic model are investigated and presented as under.

Micro-slit plate. The parametric study includes variation of thickness from 0.5 mm to 5 mm, diameter from 0.1 mm to 1 mm and slotted rate from 1% to 20% of micro-slit plate. The influence of above parameters on absorption coefficients of the bionic model are shown in Fig. 8. The results reveal that the thickness and slotted rate of micro-slit plate have notable influence on absorption coefficients of the bionic model. The peak of absorption coefficient moves slightly to low frequencies with increase in the thickness greater than 0.5 mm (Fig. 5a). However, the absorption band becomes much narrower and the acoustic absorption decreases significantly in the frequency band over 700 Hz. In case of diameter, the absorption coefficients between 600 Hz and 2000 Hz increase slightly with increase in diameter above 0.2 mm, but the absorption band becomes a little narrower. The slotted rate shows a completely opposite influence as that of thickness on absorption coefficients of the bionic model.

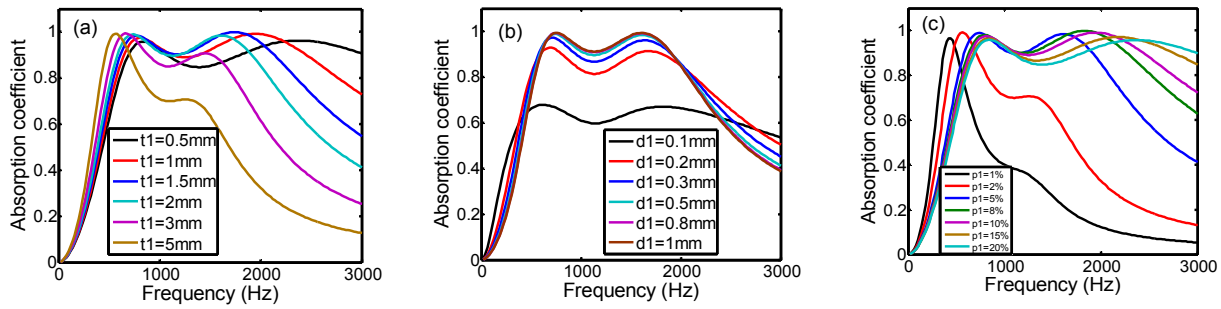

Fig. 8 Influences of (a) thickness, (b) diamater and (c) slotted rate of micro-slit plate on absorption coefficients of bionic model

Micro-perforated membrane. The parametric study includes variation of thickness from 0.05 mm to 1 mm, diameter from 0.01 mm to 1 mm and slotted rate from 0.1% to 20% of micro-perforated membrane. The influences of above parameters on the absorption coefficients of the bionic model are shown in Fig. 9. The results suggest that the influence of thickness of micro-perforated membrane is relatively smaller. As the thickness increases, the absorption coefficients at high frequencies have a tiny decrease. In case of diameter, the absorption band becomes wider and the trough of wave becomes smaller as the diameter increases from 0.01 mm to 0.1 mm. However, the peak of absorption coefficient moves to high frequencies and the values at trough of wave becomes bigger for diameter larger than 0.1 mm. The slotted rates between 0.1% - 1% have better absorption capability within the frequency band below 2300 Hz.

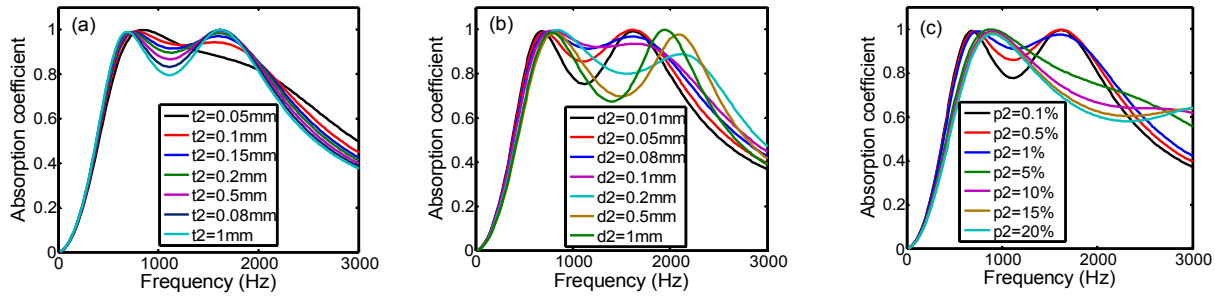

Fig. 9 Influences of (a) thickness, (b) diamater and (c) slotted rate of micro-perforated membrane on absorption coefficients of bionic model

Porous material. The resistivity of porous material varies from 2000 $Pa \cdot s / m$ to 80000 $Pa \cdot s / m$. The influence of resistivity for porous material on absorption coefficients of the bionic model is showed in Fig. 10. The results reveal that the absorption band becomes much wider with the increase of resistivity. However, the initial peak decreases significantly at low frequencies.

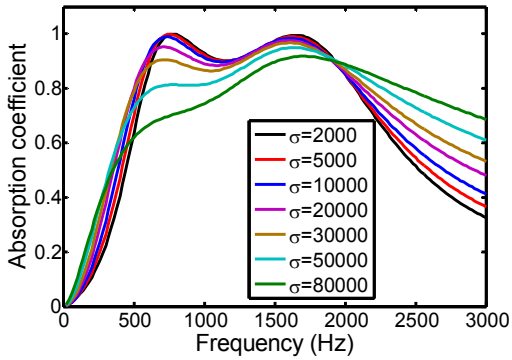

Fig. 10 Influence of resistivity of porous material on absorption coefficients of bionic model

Thickness combination of porous material and airspace. The total thickness of porous material and airspace is 50 mm. The thickness of porous material varies from 10 mm to 40 mm. The influence of thickness combination of porous material and airspace on absorption coefficients of the bionic model is presented in Fig. 11. The results demonstrate that the second peak of absorption coefficient moves to lower frequencies with the increase of porous material thickness. The value at trough of wave increases until it completely diminishes. However, the airspace thickness influences the absorption coefficient in the opposite manner.

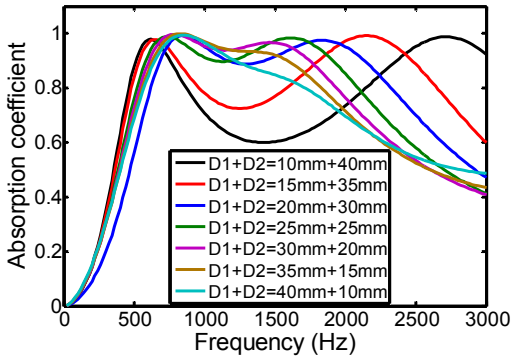

Fig. 11 Influence of thickness combination of porous material and airspace on absorption coefficients of bionic model

Conclusions

In this study, a bionic coupling multi-layer structure is developed based on the biomimetic method. The absorption coefficients and their influence factors of each layer are investigated by impedance transfer method. The bionic model shows excellent absorption performance. Its average absorption coefficient is found to be 0.778 within the frequency band of 0 to 2000 Hz while 0.85 from 200 Hz to 2000 Hz. The optimal parameters are determined as t_1=1 mm, d_1=0.5 mm, p_1=15%, t_2=0.1 mm, d_2=0.05 mm, p_2=1%, D_1=20 mm, σ =20000 $Pa \cdot s / m$, D_2=30 mm. The significant improvement of absorption coefficients at low frequencies can be mainly due to the Helmholtz effects of the micro-silt plate and flexible micro-perforated membrane, and the combination with porous materials, which leads to even better absorption performance in broadband. The study emphasizes that further investigations on the bionic coupling multi-layer structure can provide better absorbing system for practical applications.

Acknowledgments

All support is greatly acknowledged and appreciated, especially the constructive discussion and criticism from colleagues. Thanks are due to the Joint Funds of the National Natural Science Foundation of China (Grant No. U1134109), the Specialized Research Fund for the Doctoral Program of Higher Education of China (Grant No. 20110061120048), and the projects of National Natural Science Foundation of China (Grant No. 31071928, 51106062 and 51206058), for allowing to undertake the project and the financial support extended.

References

[1] C.Y. Xue, S. Chen, W.D. Zhang, B.Z. Zhang, G.J. Zhang, and H. Qiao, Design, fabrication, and preliminary characterization of a novel mems bionic vector hydrophone. Microelectronics Journal, 2007, 38, 1021–1026.

[2] Z.W. Han, S.C. Niu, C.H. Shang, Z.N. Liu, and L.Q. Ren, Light trapping structures in wing scales of butterfly trogonoptera brookiana. Nanoscale, 2012, 4, 2879–2883.

[3] L.Q. Ren, J. Tong, J.Q. Li, B.C. Chen, Swsoil and water: Soil adhesion and biomimetics of soil-engaging components: a review. Journal of Agricultural Engineering Research, 2001, 79, 239–263.

[4] T.L. Sun, L. Feng, X.F. Gao, L. Jiang, Bioinspired surfaces with special wettability. Accounts of Chemical Research, 2005, 38, 644–652.

[5] L. Feng, H.S. Li, Y.S. Li, H.J. Li, L.J. Zhang, J. Zhai, Superhydrophobic surfaces: From natural to artificial. Advanced materials, 2002, 14, 1857–1860.

[6] R.R. Graham. The silent flight of owls, The Journal of the Royal Aeronautical Society, 1934, 38, 837–843.

[7] R.A. Kroeger, H.D. Grushka, T.C. Helvey, Low Speed Aero-Dynamics for Ultra-Quiet Flight, Technical Report AFFDL-TR-71-75, Air Force Flight Dynamics Lab, Wright-Patterson Air Force Base, Ohio, USA, 1971.

[8] G.M. Lilley, A study of the silent flight of the owl. AIAA Paper, 1998, 2004–2186.

[9] G.M. Lilley, A quest for quiet commercial passenger transport aircraft for take-off and landing. AIAA Paper, 2004, 2922.

[10] S.M. Sun, L.Q. Ren, C.Y. Xun, Research on coupling sound absorption property of owl skin and feather. Noise and Vibration Control, 2008, 6, 119–123. (in Chinese)

[11] T.S. Liu, K. Kuykendoll, R. Rhew, S. Jones, Avian wings. AIAA Paper, 2004, AIAA–2004–2186.

[12] W.A. Davern. Perforated facings backed with porous materials as sound absorbers- an experimental study. Applied Acoustics, 1977, 10, 85–112.

[13] I.P. Dunnand, W.A. Davern, Calculation of acoustic impedance of multilayer absorbers. Applied acoustics, 1986, 19, 321–334.

[14] L. Jinkyo, W. George, J. Swenson, Compact sound absorbers for low frequencies. Noise Control Eng J, 1992, 38, 109–117.

[15] W.H. Chen, F.C. Lee, D. M. Chiang, On the acoustic absorption of porous materials with different surface shapes and perforated plates. Journal of sound and vibration, 2000, 237, 337–355.

[16] L. Lin, Z.M. Wang, Z.X, Jiang. Effect of sound–absorbing material on a micro-perforated absorbing construction. ACTA acoustic, 2010, 4, 385–392.

[17] D.H. Lee, Y.P. Kwon, Estimation of the absorption performance of multiple layer perforated panel systems by transfer matrix method. Journal of sound and vibration, 2004, 278, 847–860.

[18] F.C. Lee, W.H. Chen, Acoustic transmission analysis of multi-layer absorbers. Journal of Sound and Vibration, 2001, 248, 621–634.

[19] X.D. Zhao, P. Hu, P. Sun, The comparative analyses of the calculation methods for absorptivity of multilayer micro-perforated panel absorbers. Applied Acoustic, 2012, 3, 6.

[20] D.Y. Maa, Theory of microslit absorbers. Acta Acustica, 2000, 25, 481–485.

[21] Y. Miki, Acoustical properties of porous materials-Modifications of Delany-Bazley models. J. Acoust. Soc. Jpn.(E), 1990, 11, 19–24.

[22] J. Kang, H.V. Fuchs, Predicting the absorption of open weave textiles and micro-perforated membranes backed by an air space. Journal of sound and vibration, 1999, 220, 905–920.

[23] W.A. Davern, Perforated facings backed with porous materials as sound absorbers- an experimental study. Applied Acoustics, 1977, 10, 85–112.

Advances in Bionic Engineering
10.4028/www.scientific.net/AMM.461

Acoustic Performance Analysis of Bionic Coupling Multi-Layer Structure
10.4028/www.scientific.net/AMM.461.22